THE JOURNAL OF PHYSICAL CHEMISTRY C

Article

pubs.acs.org/JPCC

First-Principles-Based Reaction Kinetics for Decomposition of Hot, Dense Liquid TNT from ReaxFF Multiscale Reactive Dynamics Simulations

Naomi Rom,*[,†] Barak Hirshberg,[†] Yehuda Zeiri,[§,∥] David Furman,[†] Sergey V. Zybin,[‡] William A. Goddard, III,[‡] and Ronnie Kosloff[†]

[†]The Fritz Haber Research Center for Molecular Dynamics, Institute of Chemistry, Safra Campus, The Hebrew University of Jerusalem, Jerusalem 91904, Israel

[‡]Materials and Process Simulation Center, California Institute of Technology, 1200 East California Boulevard, Pasadena, California 91125, United States

[§]Biomedical Engineering, Ben Gurion University of the Negev, Beer-Sheva 8410501, Israel

[∥]Division of Chemistry, NRCN, P.O. Box 9001, Beer-Sheva 84190, Israel

Supporting Information

ABSTRACT: The reaction kinetics of the thermal decomposition of hot, dense liquid TNT was studied from first-principles-based ReaxFF multiscale reactive dynamics simulation strategy. The decomposition process was followed starting from the initial liquid phase, decomposition to radicals, continuing through formation of carbon-clusters products, and finally to formation of the stable gaseous products. The activation energy of the initial endothermic decomposition rate and the subsequent exothermic reactions were determined as a function of density. Analysis of fragments production in different densities and temperatures is presented. We find that unimolecular C−N bond scission dominates at the lower densities (producing NO_2), whereas dimer formation and decomposition to TNT derivatives and smaller gaseous fragments prevails at higher compressions. At higher densities, enhanced carbon-clustering is observed, while the initial gaseous fragments formation is suppressed. Increasing the temperature speeds up the production of both clusters and gaseous products. The activation energy for the initial decomposition stage of ambient liquid TNT is ∼36 kcal/mol, close to the measured value (∼40 kcal/mol). This value is ∼25 kcal/mol lower than the corresponding gas phase C−N bond scission. Finally, we suggest a simple linear growth kinetic model for describing the clustering process, which provides very good agreement with simulation results.

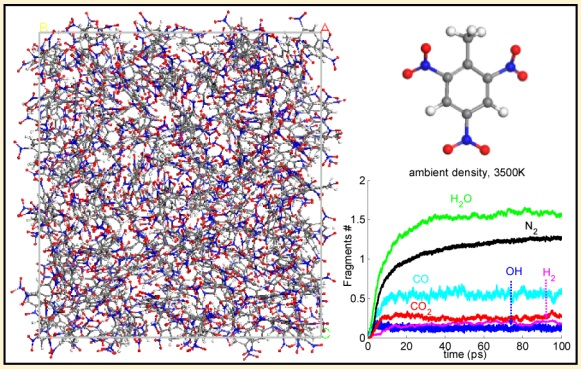

1. INTRODUCTION

Experimental techniques generally do not provide sufficient details of the reaction steps to extract the detailed reaction kinetics of decompositions of liquids or solids. Hence it would be most valuable to develop theory- and computation-based methods to extract the atomistic details of the mechanisms. First-principles quantum mechanics (QM) provides the means for extracting such atomistic details; however, it is not practical to carry out QM on sufficiently large systems and times to simulate realistic descriptions of the shock-induced transformations. A possible solution of this conundrum is reactive molecular dynamics, using the ReaxFF reactive force field adjusted to fit the bond breaking and reaction pathways to QM on model systems. ReaxFF allows molecular dynamics (MD) simulations with nearly the accuracy of QM but on the time scales of force field (FF)-based MD. In this case, the question is whether the approximations involved in ReaxFF retain a sufficiently faithful description of the QM that enables us to obtain quantitatively accurate descriptions of the shock-induced chemistries. This paper validates that ReaxFF does indeed provide this level of accuracy for a moderately complex system liquid trinitrotoluene (TNT, $C_7H_5N_3O_6$).

TNT is an insensitive high explosive (HE) with a wide range of applications. Because of its low melting point (80 °C), it can be cast in various shapes and mixed with other materials to make composites. The study of liquid TNT initiation focuses on the kinetic processes involved, without the influence of solid explosive characteristics (e.g., grain boundaries).

Received: May 19, 2013
Revised: August 24, 2013
Published: September 11, 2013

The unimolecular dissociation reactions of TNT have been calculated[1] using density functional theory (DFT). Three initial reaction routes were identified:

(1) NO_2 homolysis
(2) C−H alpha attack, leading to the formation of 2,4-dinitroanthranil and water molecule release
(3) NO_2−ONO rearrangement

The detailed chemical mechanisms were elucidated in ref 1, elaborating on the intermediate species along these reaction paths as well as the free energies and enthalpies in the temperature range of 300−3500 K. At room temperature the kinetically and thermodynamically favorable unimolecular path found was the C−H alpha attack, whereas at 3500 K the NO_2 homolysis was dominant. The calculated free energies for reactions 1−3 at 300 K are[1] 43.8, 37.7, and 54.9 kcal/mol, respectively, whereas at 3500 K the corresponding values are −90.6, 60.8, and 60.1 kcal/mol.

The decomposition of liquid TNT can possess various mechanisms differing from the unimolecular ones, in particular, binary reactions and other many-body effects. A density-dependent initial decomposition mechanism was also found for hot and dense nitromethane (NM) using ReaxFF MD simulations.[2] In the NM case, a change of mechanism was found from unimolecular to bimolecular at high temperature and compression.

Molecular dynamics (MD) simulations were performed to study these decomposition pathways in liquid TNT. These calculations were done under hydrostatic compression as a function of density at high temperatures. The LAMMPS molecular dynamics simulation package[3] was employed with ReaxFF potentials[4,5] including low gradient (LG) dispersion correction.[6] The evolution of fragments that were formed during the decomposition process of liquid TNT was revealed, and the corresponding reaction kinetics parameters were evaluated.

Unique to TNT decomposition is the generation of soot under reaction/explosion conditions.[7] This is partially due to the low oxygen content of TNT. The formation of soot is also common in other HE nitroaromatic substances, such as 1,3,5-triamino-2,4,6-trinitrobenzene (TATB), and was obtained in previous ReaxFF-MD simulations.[8] The present liquid TNT simulations are able to follow the soot formation, represented by the formation of large, carbon-rich clusters. An analysis of the clusters production process suggests a kinetic model that describes the coagulation mechanism.

The computational approach is described in Section 2, and the results of the simulations are presented in Section 3. The decay of liquid TNT at high temperatures and compressions is shown and analyzed, starting at the initial decomposition, followed by intermediate fragments formation and finally stable products formation. The clusters analysis and the kinetic model are presented in Section 4, and the conclusions are summarized in Section 5.

2. COMPUTATIONAL APPROACH

The decomposition of liquid TNT was simulated using molecular dynamics with LG-corrected[6] ReaxFF potentials[4,5] implemented in the LAMMPS code.[3]

The potential parameters are presented in Section 5 in the Supporting Information (SI). The approach is verified in Section 2.1, where the enthalpy change calculated with these ReaxFF potentials is compared with DFT values for two TNT unimolecular decomposition paths.

The ReaxFF-MD simulation cell includes 288 TNT molecules (6048 atoms). The liquid sample preparation, heat-up simulations, and the decomposition and kinetic analyses follow the schemes of ref 2, where the decomposition of hot, dense liquid NM was studied using ReaxFF MD simulations. For comparison, an additional liquid phase was generated from an amorphous random sample. New techniques were required for the analysis of the clusters formation in liquid TNT decomposition, which are not relevant to NM decomposition. Thus, only the main points that are typical to the present liquid TNT simulations are described in the sections below.

2.1. Single TNT Molecule Decomposition. The decomposition paths of a single TNT molecule were studied intensively using DFT (see, for example, refs 1 and 9). Two unimolecular reactions of TNT were chosen as benchmarks to validate the ReaxFF potentials. The enthalpy change values calculated using DFT are compared with ReaxFF potentials. The enthalpy change values calculated using DFT are compared with ReaxFF potential energies in LAMMPS:

(1) $C_7H_5N_3O_6$ (TNT) → $C_7H_5N_3O_6$ (ortho-nitril (ONO)−TNT, see Figure 1)

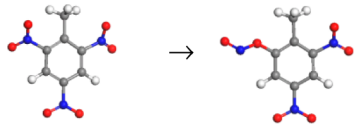

Figure 1. NO_2 → ONO (nitro-nitril) rearrangement in TNT molecule.

(2) $C_7H_5N_3O_6$ (TNT) → $C_7H_5N_2O_4$ + NO_2 (NO_2 homolysis)

The enthalpy change in these reactions is obtained from the potential energy (PE) difference at 0 K between the initial TNT molecule and the energy-minimized products. The enthalpy change obtained using ReaxFF potentials for equations 1 and 2 above is −1.2 and 61.4 kcal/mol. The DFT results at 298 K are −6.6 (−8.1) and 57.0 (58.0) kcal/mol in ref 9 (ref 1), respectively. The ReaxFF parameters can be further optimized for improved description of TNT decomposition energetics; however this is not within the scope of this paper.

In Section 3.2, the activation energy of the initial decomposition step of liquid TNT is calculated.

2.2. Sample Preparation. The unit cell used for the liquid TNT simulation cell preparation is[10] CSD_CIF_ZZZMUC01, with a, b, c = 14.991, 6.077, 20.017 Å. (See Figure 2.) First, a 3 × 6 × 2 expanded crystal supercell was created, and its energy was minimized. (See Figure 2, middle.) The orthorhombic supercell lattice vectors are: a, b, c = 44.730, 36.204, 39.360 Å. Thereafter, the following procedure was applied:

- The supercell volume was increased by 45% (enabling TNT molecules mobility upon heating); then, its energy was minimized, resulting in an optimized geometry.
- This supercell was slowly heated to 500 K (well above the TNT melting point, 354 K), for a duration of 10 ps. Note that an additional thermalization stage at 500 K for 20 ps did not cause a significant change in the results shown below.
- The hot cell was heavily compressed (NPT simulation at 1 GPa and 500 K, for 30 ps).
- Cooling and decompression was applied (NPT simulation at 1 atm and 400 K, for 30 ps). The calculated mass density of the liquefied sample at the end of the simulation was

dx.doi.org/10.1021/jp404907b | J. Phys. Chem. C 2013, 117, 21043−21054

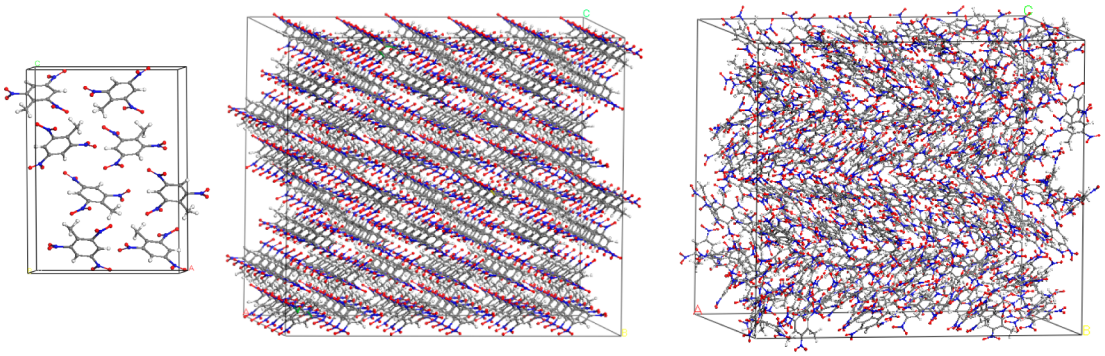

Figure 2. TNT orthorhombic unit cell[10] (left). Energy-minimized TNT crystal supercell (middle). Liquid simulation cell at 1 atm, 400 K (right).

1.444 g/cm^3 (a, b, c = 47.2714, 38.2609, 41.5961 Å), in excellent agreement with the measured density[11] at 373 K: 1.443 g/cm^3.

- The liquid cell was then thermalized (NVT simulation at T = 400 K, for 2 ps).
- Finally, the system state was relaxed (NVE simulation, for 1 ps). A typical liquid supercell is shown in Figure 2 and Figure 1 in the SI. It can be seen that some long-range order remains in the liquid cell.

The time step used in the procedure described above was 0.25 fs.

The influence of the liquid preparation scheme on its structure and thermal decomposition was checked by constructing an amorphous TNT liquid using the scheme outlined in Section 1 in the SI. A comparison between the radial distribution function (RDF) of the solid TNT and the liquid cells, prepared from crystal (denoted *liquid 1*) and from amorphous TNT molecules (*liquid 2*), is presented in Figure 3. *Liquid 1* RDF has smooth,

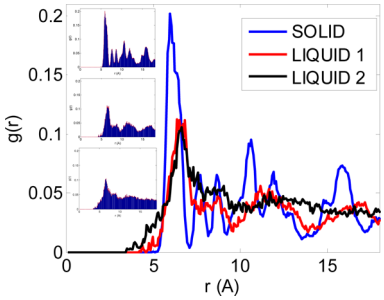

Figure 3. Radial distribution functions (RDFs) for solid TNT (300 K, blue) and liquid TNT at 400 K prepared from crystal (*liquid 1*, red) and amorphous (*liquid 2*, black) cells. The inserts are the separate RDFs for the solid (top), *liquid 1* (middle), and *liquid 2* (bottom). Distance units are angstroms.

smeared peaks that are characteristic of a liquid phase, but some order is preserved in the vicinity of the crystal sharp peaks. This order is in contrast with the simple NM liquid cell constructed using a similar scheme, where long-range order was absent.[2] Liquid TNT is more complex, and the remaining order can result from intermolecular hydrogen bonding between NO_2 groups in one TNT molecule and hydrogen atoms in adjacent ones.[12] This effect can be more pronounced in the vicinity of the melting point. The RDF of liquid 2 is smoother, and the long-range structure seen in liquid 1 is smeared.

Despite the long-range order remaining in TNT *liquid 1*, the decomposition and kinetics at high temperatures are only slightly affected by the initial liquid structure, as shown in SI Section 1. Thus, all of the results reported herein are calculated on TNT *liquid 1* system.

2.3. Liquid Compression. The initial liquid sample prepared by the process described above (at 400 K and 1 atm) was volumetrically compressed by the desired amount to obtain a liquid phase at various compressions. Then, the compressed liquid cell energy was minimized until equilibrium positions were obtained. Finally, each compressed liquid cell was thermalized using NVT simulation at 400 K for 5 ps. It is important to note that none of the TNT molecules decomposed during these initial state preparation stages.

The liquid TNT densities obtained are shown in Table 1, corresponding to ambient density, 15 and 30% compression at 400 K.

Table 1. Densities, Volumes, and Compressions of the Heat-Up Simulation Cells

mass density [g/cm^3]	cell volume, V [Å^3]	compression, V/V_0
1.444	75 233	1
1.699	63 948	0.85
2.063	52 663	0.7

2.4. Heat-Up Simulations. Liquid TNT heat-up simulations were carried out in two stages: Initially, the sample at a fixed density was heated rapidly (within 100 fs, using time step 0.1 fs) from the initial liquid temperature of 400 K to the desired temperature (T_f). Then, NVT simulations were carried out at T_f until the final decomposition products were obtained. The values of T_f used are: 1800, 2250, 2700, and 3500 K.

The rapid heating is carried out on a time scale similar to that of a detonation wave passing through the simulation cell (~500 fs). The measured detonation velocity of liquid TNT with initial density 1.472 g/cm^3 is[13] 6.633 ± 0.012 km/sec, and the Chapman Jouguet pressure is[14] 182 ± 12 kbar. The time step used in the NVT simulations was 0.25 fs. (The energy conservation is similar for simulations with 0.1 and 0.25 fs time steps.) The simulations length varied between 100 and 200 ps depending on the reaction rate.

2.5. Thermal Kinetic Analysis. Fragments formation along the liquid TNT decomposition path is analyzed using an internal code from the LAMMPS package[3] in the following regimes:

- Initial decomposition (endothermic stage)
- Intermediate reactions and products (exothermic stage)
- Final products formation
- Gaseous products: H_2O, CO_2, N_2, H_2, NH_3, CO, and OH
- Soot (large clusters)

dx.doi.org/10.1021/jp404907b | J. Phys. Chem. C 2013, 117, 21043−21054

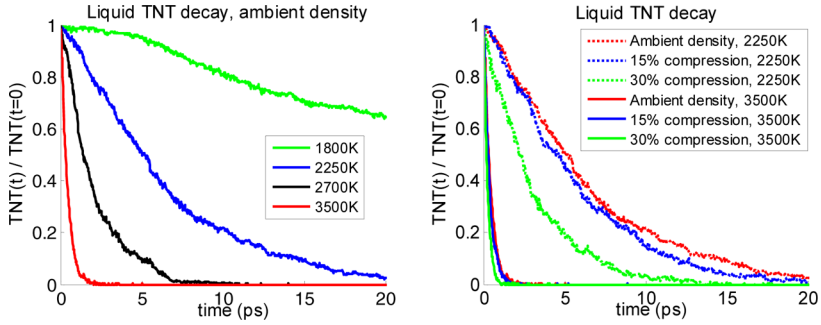

Figure 4. Decay of liquid TNT versus simulation time at (1) ambient density and various temperatures (left) and (2) various compressions and 2250 and 3500 K (right).

The liquid TNT decomposition thermal rate constants for the initial and intermediates stages and for the gaseous products formation stages, were calculated using the formalism outlined in the study of liquid NM[2]. The soot formation kinetic analysis was carried out using a linear growth model, as described in Section 4.3.

3. RESULTS: GASEOUS FRAGMENTS FORMATION AND THERMAL RATE CONSTANTS

The decomposition of liquid TNT and the gaseous products formed in ReaxFF-MD simulations under extreme conditions are now presented. Thermal rate constants are computed for the decomposition reaction in the initial and intermediate stages from the TNT decay (k_1) and the PE decay (k_2). In particular, the influence of compression and temperature on the above decomposition is studied. The calculated total pressure and PE in these simulations are presented in Section 2 in the SI.

3.1. Liquid TNT Initial Decay. The time evolution of the amount of TNT molecules, normalized by the initial number of molecules, is presented in Figure 4 for various temperatures and densities. The initial, rapid heating stage is not shown in these plots, and it was verified that no decomposition occurred during this period. As seen (Figure 4, right), the decomposition rate increases when density (compression) increases. The reaction rate increase with compression is expected if the decomposition dynamics is dominated by intermolecular processes. In contrast, the increase in liquid TNT decomposition rate due to temperature increase (Figure 4) is expected in both unimolecular and bimolecular reactions because the probability to overcome energy barriers is higher at elevated temperatures. These findings are further discussed in Section 3.3 in relation to the fragments formation under the various conditions.

3.2. Decomposition Reactions Rate Constants: k_1 and k_2. Rate constants for the initial (k_1) and intermediate (k_2) decomposition stages were calculated by the procedure described in ref 2. The first step in the analysis is finding t_{max}, the time when the maximum value of PE is reached (see SI Figure 12). k_1 is obtained by fitting an exponential decay function to the TNT decay curve in the range $[t_0,t_{max}]$, where t_0 is the time when decomposition begins. (Note that t_0 is not necessarily the time when the fast heating stage ends.) The value of k_2 is obtained by fitting an exponential decay function to the PE decay in the range $[t_{max},t_{end}]$, where t_{end} denotes the time when all TNT molecules decomposed. As seen in Figure 5, t_{max} decreases with increased compression and temperature, in correlation with the increase in the reaction rate. Note that at the lower temperatures the PE has a flat top (see SI Figure 12), which reduces the accuracy of t_{max}.

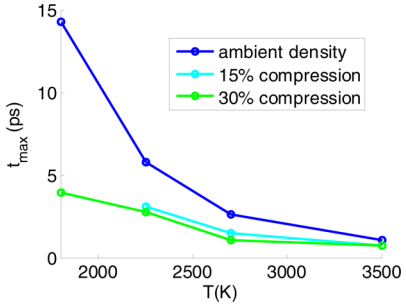

Figure 5. Plot of PE maximum time, t_{max} (ps) versus temperature (K), for ambient density, and 15 and 30% compressed liquid TNT.

Arrhenius plots of the rate constants for the initial and intermediate decomposition stages of liquid TNT are shown in Figure 6. The Arrhenius parameters for k_1 and k_2 are summarized

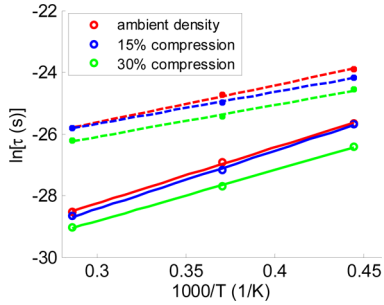

Figure 6. Arrhenius plots (shown is reaction time, $\tau = 1/k$) for liquid TNT decomposition: (1) initial, endothermic stage (k_1, full lines) and (2) exothermic reactions stage (k_2, dashed lines), for various densities in the temperature range 2250−3500K.

in Tables 2 and 3, respectively. Both reaction rates increase for higher values of temperature and compression at the studied ranges. However, it is seen that the activation energy (E_{a1}) of the

Table 2. Arrhenius Parameters Fitted to TNT Exponential Decay Rates, $k_1[\rho,T]$, over $[t_0,t_{max}]$ Time Interval for Various Initial Compressions (see the corresponding densities in Table 1)[a]

compression, V/V_0	$\ln(A_0[\mathrm{sec}^{-1}])$	E_{a1} [kcal/mol]
1	33.7	35.8
0.85	34.1	37.3
0.7	33.8	32.7

[a]Temperature range used: 2250−3500 K.

dx.doi.org/10.1021/jp404907b | J. Phys. Chem. C 2013, 117, 21043−21054

Table 3. Arrhenius Parameters Fitted to Potential Energy Exponential Decay Rate, $k_2[\rho,T]$, over $[t_{max},t_{end}]$ Time Interval for Various Initial Compressions[a]

compression, V/V_0	$\ln(A_0[sec^{-1}])$	E_{a2} [kcal/mol]
1	29.2	24.0
0.85	28.8	20.5
0.7	29.2	20.5

[a]Temperature range used: 2250−3500 K.

initial decomposition stage is similar for ambient density and 15% compression cases (the latter is higher by only ∼4%), while for 30% compression E_{a1} is lower by ∼10%. This nonmonotonic behavior can be explained by an initial decomposition mechanism change that occurs when compression increases from lower compressions to 30%. This point will be further discussed in Section 3.3.

The calculated activation energy of ambient density liquid TNT is ∼36 kcal/mol. (See Table 2.) This value is close to the one obtained using ESR techniques for the thermal decomposition of liquid TNT:[15] 40.9 ± 1.6 kcal/mol. As seen in Section 3.3, the initial process in the thermal decomposition of ambient density liquid TNT is NO_2 cleavage, for which the unimolecular enthalpy change with ReaxFF is 61.4 kcal/mol. Thus, the NO_2 homolysis barrier is ∼25 kcal/mol higher in the gas phase than in the liquid. This finding supports a radical mediated mechanism that was recently found in nitrobenzene and nitrotoluene C−N bond cleavage.[16] In this case, the bond dissociation energy in the radical anions was 23 kcal/mol below the gas-phase value.

The activation energies obtained using ReaxFF-MD for the liquid and the solid phases of TNT[17] are similar under the studied conditions.

An effective overall first-order decay rate of liquid TNT can be obtained by fitting an exponential decay function to the whole range of TNT decomposition $[t_0,t_{end}]$. The Arrhenius plot is shown in Figure 7, compared with the TNT decay rate fitted in

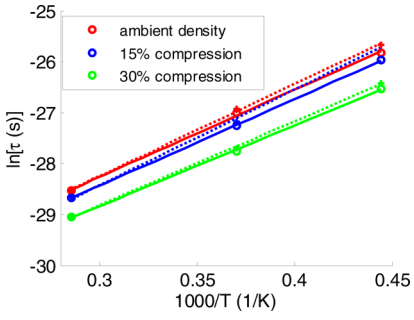

Figure 7. Arrhenius plots (shown is reaction time, $\tau = 1/k$) for liquid TNT initial decomposition (k_1) for two cases: exponential fit is carried out in the region $[t_0,t_{max}]$ (dotted lines, +) and $[t_0,t_{end}]$ (full lines, ○) for various densities in the temperature range 2250−3500 K.

the range $[t_0,t_{max}]$. The Arrhenius parameters for this effective decay rate are presented in Table 4. The calculated effective activation energy (E_{a1}) for the ambient density liquid TNT, 34 kcal/mol, is very close to the measured value based on the *total* reaction time in liquid TNT thermal decomposition ESR measurements,[15] 32.3 ± 0.9 kcal/mol. The effective decay rate is *faster* than the one obtained with the endothermic stage only, in all compressions, as can be expected when additional reactions contribute and speed up the TNT decay. In addition, the nonmonotonic activation energy change with compression seen

Table 4. Arrhenius Parameters Fitted to TNT Exponential Decay Rates, $k_1[\rho,T]$, over the Region $[t_0,t_{end}]$ for Various Initial Compressions[a]

compression, V/V_0	$\ln(A_0[sec^{-1}])$	E_{a1} [kcal/mol]
1	33.4	34.0
0.85	33.5	33.7
0.7	33.6	31.4

[a]Temperature range: 2250−3500 K.

in the endothermic-stage-only case (Table 2) is absent in the case of the effective first order decay rate constant (Table 4). This can be understood as the latter is less sensitive to a possible mechanism change in the initial decomposition stage or to a nonmonotonic reactant decay curve. In the case of liquid NM[2], the activation energy calculated in the range $[t_0,t_{max}]$ was higher by up to 12% from the one calculated between $[t_0,t_{end}]$ for densities above 30% compression. This is related to a change in the *initial* decomposition mechanism of NM decay when compression increases, which is averaged out when the exponential function fit to the reactant decay is done over the whole decomposition period.

The kinetic values suggest an estimate of the temperatures for which liquid TNT decomposition is significant. Rates in the vicinity of $k_1 = 1$ Hz ($\tau = 1$ s) are obtained by interpolating the Arrhenius plot (Figure 6). The temperatures obtained are 530, 550, and 490 K for 0, 15, and 30% compressions, respectively. This implies that when confined TNT is heated to temperatures above ∼500 K (where TNT is a liquid) it starts to decompose within a time scale of ∼1 s. Similarly, for $k_1 = 0.001$ Hz, the corresponding interpolated reaction temperatures are 675, 690, and 615 for 0, 15, and 30% compressions.

3.3. Fragments Analysis: Initial and Intermediate Reactions. The fragments formed in the heat-up simulations of liquid TNT were obtained using the fragments analysis code supplied in LAMMPS.[3] The fragments are identified according to the bond order calculated for each pair of atoms with ReaxFF potentials and the bond-order cutoff values used in the fragments analysis code. (See Section 3 in the SI.)

The stable products and soot that are produced in later stages of the simulation are analyzed separately in Sections 3.4 and 4.

The *initial* fragments formed are presented for ambient density and 30% compression at the two extreme temperatures studied (1800 and 3500 K) in Figures 8 and 9. Plots of the initial fragments formed at 2250 and 2700 K at these densities appear in SI Figures 15−17 (Section 4 therein). Only the fragments that reach >2% of the initial amount of TNT molecules (288) during the simulations are shown. Also marked is t_{max}, the exothermic reactions initiation time. Several observations that can be deduced from the plots are:

(1) At $T = 1800$ K: The initial decomposition step involves TNT-dimer ($C_{14}H_{10}O_{12}N_6$) creation, followed by its instant decomposition, producing the fragments NO_2, $C_7H_5O_5N_3$, and $C_7H_5O_5N_2$. (See the initial fragmentation in Figure 8.) The amount of these fragments is similar for some period, indicating that they are formed concurrently, via the dimer decomposition reaction. The amount of dimers is very low, which means that its stability is low at 1800 K. Note that the length of the correlation between the fragments creation depends on the density: At ambient density this decomposition route lasts for ∼25 ps (Figure 8, left), whereas with 30% compression the correlation is interrupted after ∼2.5 ps (Figure 8, right). The correlation ends when other reactions initiate, interfere, and compete with this

dx.doi.org/10.1021/jp404907b | J. Phys. Chem. C 2013, 117, 21043−21054

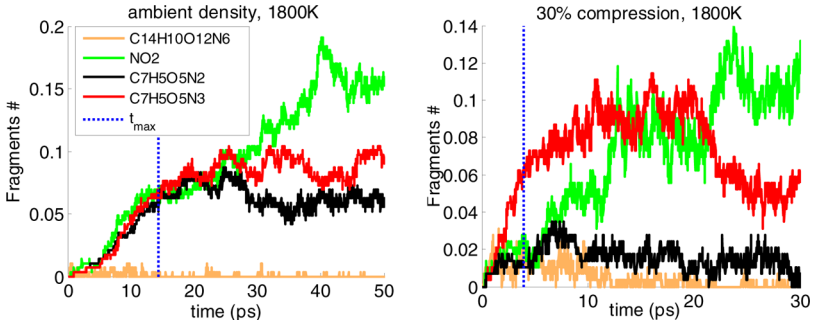

Figure 8. Comparison between the initial fragments created at ambient density and 30% compression at 1800 K.

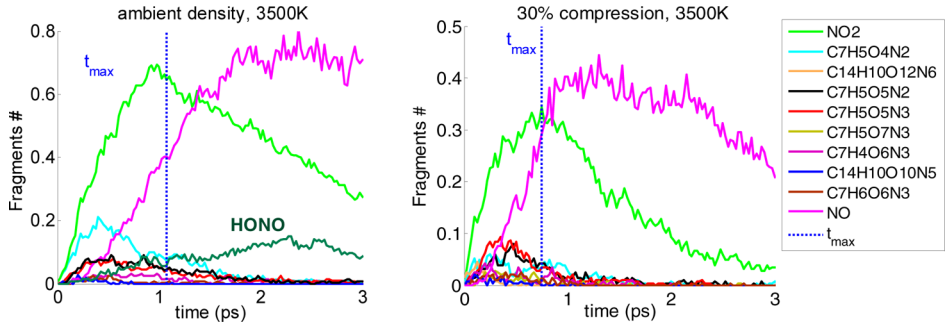

Figure 9. Comparison between the initial fragments created at ambient density (left) and 30% compression (right) at 3500K.

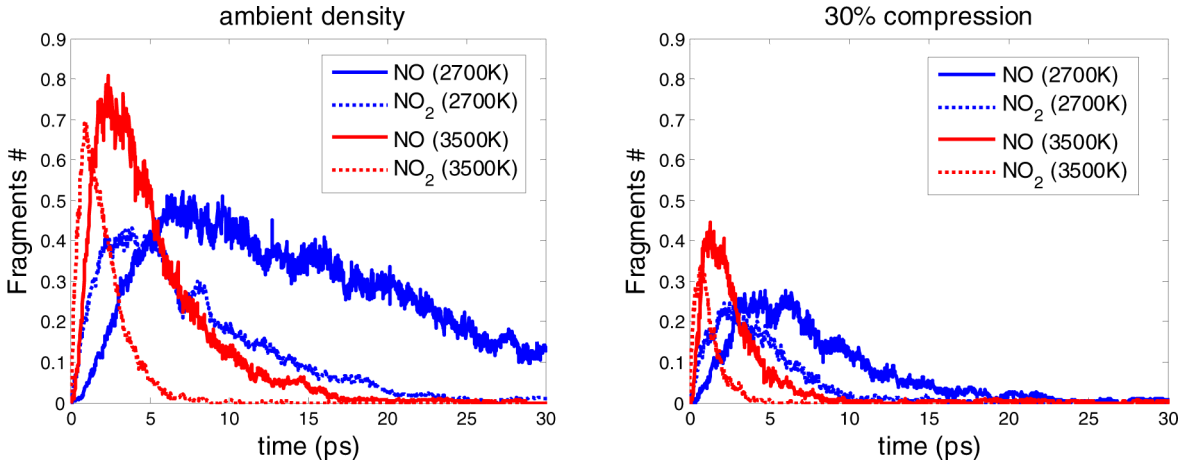

Figure 10. NO and NO_2 formation at ambient density (left) and 30% compression, at 2700 and 3500 K.

initial reaction path. In SI Figure 14 (Section 4 therein), additional initial fragments are shown (TNT derivatives and NO). At the higher compressions, the fragment variety and amount increase.

(2) At ambient density and temperature >1800 K: The initial reaction is a unimolecular decomposition of a TNT molecule via C−N bond scission (see green and cyan lines in SI Section 4, Figures 15 and 16). After some delay, the TNT-dimer ($C_{14}H_{10}O_{12}N_6$) is formed and decomposes, via the route described above, to the fragments NO_2, $C_7H_5O_5N_3$, and $C_7H_5O_5N_2$ (see green, red, and black lines in SI Section 4, Figures 15 and 16).

(3) At 30% compression and temperature range 1800−3500 K: Initially the TNT-dimer is formed (see SI Section 4, Figure 15). Then, it decomposes to various TNT and TNT-dimer derivatives and smaller fragments. The major small molecular fragments formed in this stage are NO_2 (of which only a small part is created by a unimolecular C−N bond break in a TNT molecule) and NO, and the dominant TNT derivative is $C_7H_5O_5N_3$. As temperature increases, the variety of derivatives increases.

(4) At 30% compression and temperature ≈ 3500 K: The unimolecular decomposition via C−N bond scission becomes energetically favored at this high temperature and density and begins the decomposition process of liquid TNT under these conditions. It is closely followed by the dimer creation and decomposition reactions as well as other TNT derivatives formation.

As described in Section 3.2, the activation energies for the initial decomposition stage of liquid TNT demonstrate a nonmonotonic behavior when compression increases beyond 15%. (See Table 2.). The fragments analysis previously discussed supports this behavior for $T \geq 2250$ K: The initial decomposition reaction of ambient and moderate densities liquid TNT (≤15%

dx.doi.org/10.1021/jp404907b | J. Phys. Chem. C 2013, 117, 21043−21054

compression; fragments for this case are not shown) is the unimolecular C−N bond scission, whereas for high compressions (≥30%), below 3500 K, the decomposition begins with TNT dimer formation and decomposition, accompanied by NO_2 release. Apparently, the activation energy for the latter initial decomposition process is lower by ∼10%.

Comparing the behavior of liquid and gas TNT, it is seen that the unimolecular NO_2 scission is a common initial decomposition mechanism for both gas-phase and liquid TNT at lower compressions (≤15%) and T > 1800 K. However, at lower temperatures, the initial decomposition process in the gas phase is the C−H alpha attack,[1] whereas for liquid TNT the dimer formation and decomposition is favored (at all compressions studied). In addition, in contrast with the gas-phase and low-density liquid TNT initial reactions, the initial decomposition path of 30% compressed liquid TNT in the temperature range 1800−3500 K is dimer formation and decomposition.

The following observations arise when comparing the liquid and solid[17] TNT decomposition:

(1) At low temperatures, TNT dimer formation is the first step in the bulk TNT thermal decomposition. In the liquid, the dimer amount is smaller and it decomposes faster (i.e., less stable), producing initially mainly NO_2, $C_7H_5O_5N_3$, and $C_7H_5O_5N_2$ at ambient density and mainly $C_7H_5O_5N_3$ (accompanied by additional fragments) at 30% compression. In the solid, however, the dimer formation is followed by unimolecular NO_2 homolysis at ambient density and dimer fragmentation to $C_7H_4O_6N_3$ and $C_7H_6O_6N_3$ at high compression.

(2) At high temperatures, in both the solid and the liquid, initially there is a competition between unimolecular homolysis and dimer decomposition. Note that in the solid TNT decomposition at ambient density the fragments NO and $C_7H_5O_5N_2$ are produced simultaneously, similar to the gas-phase path following NO_2−ONO rearrangement. (See figure 4 in ref 1.)

In Figure 10, the production of NO_2 and NO is shown for ambient density (left) and for 30% compression (right) at two temperatures. Under all conditions, first NO_2 is formed, thereafter NO. It can be seen that temperature speeds up these small fragments formation, while compression suppresses it. This tendency is in agreement with the enhanced clustering that takes place at high densities, along with reduction in gaseous fragments production, as will be shown in the clusters analysis in Section 4.

3.4. Final Gaseous Products Analysis: Formation and Asymptotic Amounts. The main final gaseous products obtained in the thermal decomposition of liquid TNT are: N_2, H_2, H_2O, CO_2, CO, NH_3, and OH. In Table 5, these fragments asymptotic amounts are given at 3500 K, and their temporal evolution is shown in Figure 11 under various conditions.

The final amounts of H_2O and N_2 are not very sensitive to the liquid compression. (See Figure 12.) The amount of CO_2 and CO reduces with increasing hydrostatic pressure due to the density-enhanced carbon-clustering. (See Section 4.) The temperature increase accelerates the OH and CO production. A similar result was seen in the solid TNT analysis.[17]

The density dependence of the asymptotic amount of the stable gaseous products at 3500 K is presented in Figure 12, in comparison with the measured values in confined experiments.[18] A good agreement is obtained for N_2 and H_2O. The amount of carbon-containing gases (CO and CO_2) differs from the measured values (which are higher than the calculated ones) and so do H_2, NH_3 and OH. There are several possible explanations to this disagreement. Two main issues are: (1) The pressure and temperature conditions are not identical in the experiment and the simulations and (2) ReaxFF potentials were not trained or tested for the soot formation process of liquid/solid TNT. The clusters formation directly influences the amount of carbon-containing gaseous produced and also the amount of hydrogen-containing gases, whose amount depends on the trapping (or caging) of hydrogen atoms within the clusters.

Table 5. Final Gaseous Products Asymptotic Amounts at 3500 K and Various Densities[a]

fragment	ambient density	15% compression	30% compression
OH	0.13	0.18	0.27
H_2	0.19	0.07	0.03
H_2O	1.57	1.72	1.66
CO	0.55	0.29	0.09
N_2	1.21	1.27	1.25
CO_2	0.27	0.23	0.15
NH_3			0.04

[a]Values are normalized with respect to the initial amount of TNT molecules.

4. RESULTS: SOOT FORMATION

Carbon clusters formation under pressure and during detonation of HEs has been the topic of several theoretical and experimental studies in the past years.[8,19−23] This soot formation is important because it may have a significant effect on the detonation performance of different explosives, especially ones with negative oxygen balance.[8] Despite the interest, the microscopic details of carbon clustering are yet to be resolved.

To study the time-dependent clustering in liquid TNT, we analyze the time evolution of the average molecular weight (AMW) of clusters with a number of carbon atoms (C) above a minimal value n ($C \geq n$). The AMW is defined as follows:

$$\mathrm{AMW}(t; n) = \frac{\sum_{i \in C \geq n} \mathrm{MW}_i N_i(t)}{\sum_{i \in C \geq n} N_i(t)}$$

MW_i is the molecular weight of fragment i, and $N_i(t)$ is the number of fragments of type i at a given time, t. The temporal dependence of the AMW during the simulation at 2250 K is shown in Figure 13 for the cases $C \geq 0$, $C \geq 7$, $C \geq 14$, and $C \geq 21$ and two densities (ambient and 30% compression). In all plots below, the AMW is *normalized* to the molecular weight of TNT. The $C \geq 0$ case corresponds to averaging the MW of all fragments in the simulation cell at each time step. The AMW for $C \geq 7$, $C \geq 14$, and $C \geq 21$ is calculated by averaging over the MW of fragments with at least 7, 14, and 21 carbon atoms (corresponding to TNT molecules and their derivatives, TNT dimers and their derivatives, and trimers and their derivatives, accordingly).

Each type of AMW provides both unique and complementary information:

(1) The AMW of *all* fragments ($C \geq 0$) in the simulation cell decreases as a function of time due to the formation of many small fragments (see Section 3.3).

(2) The time dependence of the AMW of all fragments with $C \geq 7$ initially decreases due to the detachment of small fragments (e.g., NO_2 and OH) from the original TNT molecules. Thereafter (at ∼10 ps, in the case shown in Figure 13 at ambient density), the AMW starts to increase due to initiation of carbon

dx.doi.org/10.1021/jp404907b | J. Phys. Chem. C 2013, 117, 21043−21054

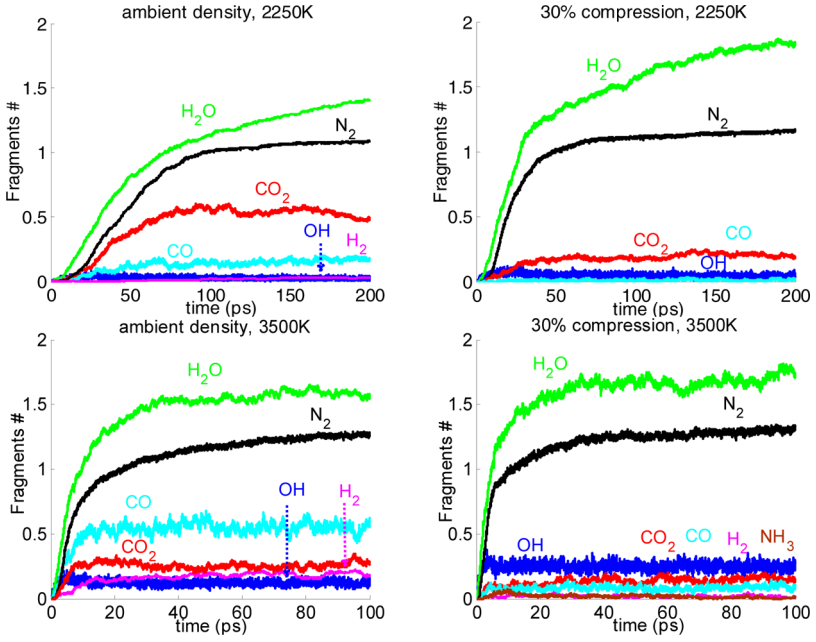

Figure 11. Final gaseous products creation at 2250 and 3500 K for ambient density and 30% compression.

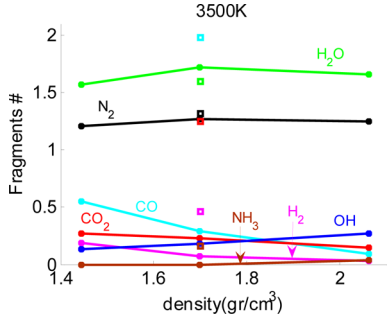

Figure 12. Final gaseous products are plotted as a function of density for liquid TNT decomposition at 3500 K. For comparison, the measured fragments from confined experiments[18] are marked (squares) using the same color code.

clustering. This process is density/pressure- and temperature-dependent, as shown below.

(3) For AMW with larger clusters ($C \geq 14$, $C \geq 21$), it is seen that they are starting to form at time $t_{form} > 0$, and they continue to grow as the simulation progresses. As can be expected, t_{form} is shorter as the minimal cluster size in the AMW calculation is smaller. Once formed, the clusters grow in a similar fashion regardless of their size.

It appears that the clusters grow in a stepwise fashion. See in Figure 13 (left) the vertical dashed lines marking the steps in AMW for $C \geq 14$ and $C \geq 21$ at ~80 and ~190 ps. At each step, the clusters grow by approximately a single TNT molecule. This observation will serve as the basis for the kinetic model presented in the following section.

Figure 13 also shows (right) the time evolution of the AMW for 30% compression. A detailed analysis of the pressure influence on the carbon clustering is discussed in Section 4.2. A few observations can be made here: Until ~20 ps, the temporal change of AMW is similar to the ambient density case for $C \geq 0$, $C \geq 7$, $C \geq 14$, and $C \geq 21$. However, unlike the ambient density results, at 30% compression, the AMW for $C \geq 7$, $C \geq 14$, and $C \geq 21$ begins to oscillate after clustering begins. In addition, the AMW for $C \geq 0$ and 30% compression shows a nonmonotonic decay starting at ~20 ps as well (see insert plot in Figure 13). The oscillations are caused by the instability of the large clusters formed, which can be an artifact of the numerical fragments

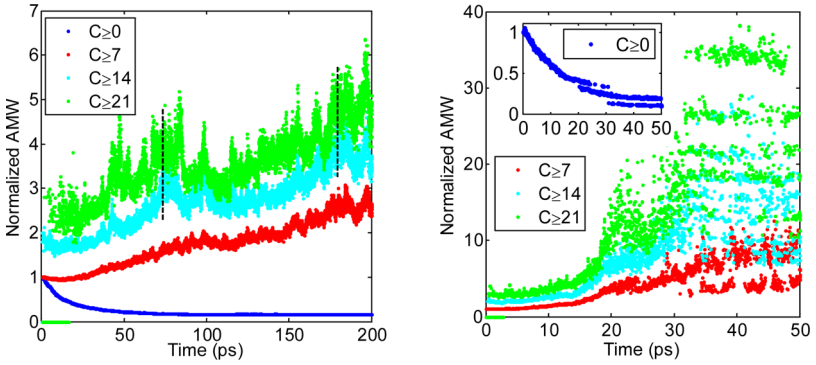

Figure 13. Average molecular weight (AMW) as a function of time for fragments with at least C carbon atoms, where $C \geq 0$, $C \geq 7$, $C \geq 14$, and $C \geq 21$. The liquid TNT simulations were done at 2250 K for ambient density (left) and 30% compression (right). The inner panel (right) shows results for $C \geq 0$ on a different scale for clarity.

dx.doi.org/10.1021/jp404907b | J. Phys. Chem. C 2013, 117, 21043−21054

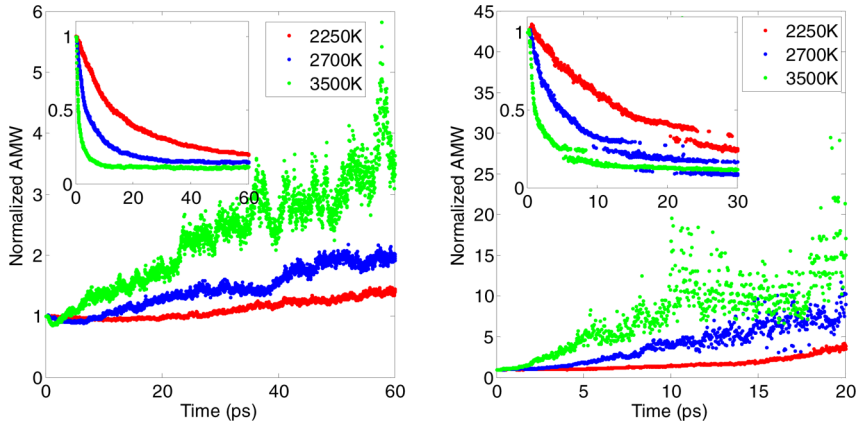

Figure 14. AMW as a function of time at ambient density (left) and 30% compression (right) at 2250, 2700, and 3500 K. The results in the main and internal panels are for $C \geq 7$ and $C \geq 0$, respectively.

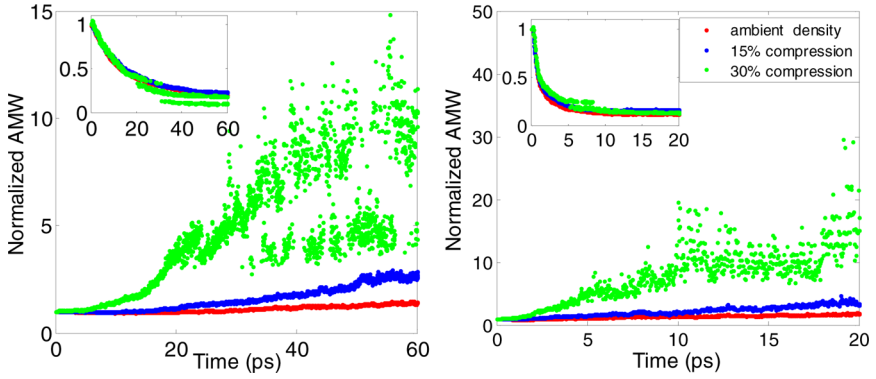

Figure 15. AMW as a function of time at 2250 (left) and 3500 K (right) for ambient density (red) and 15 (blue) and 30% (green) compressions. The results in the main and the internal panels are for $C \geq 7$ and $C \geq 0$, respectively.

analysis algorithm (not using time-window to average over unstable fragments).

To have a complete understanding of carbon clustering, it is important to analyze the effect of pressure and temperature on the clusters' growth. It is possible that different pressure and temperature conditions accelerate or decelerate the clustering or might even result in different mechanisms governing the overall clustering process.

4.1. Temperature Effect on Clustering. Figure 14 (left) shows the effect of temperature on the AMW at ambient density, for the $C \geq 0$ and $C \geq 7$ cases. In the former, it is seen that the temperature accelerates the decay in the overall AMW, as expected. For the $C \geq 7$ case, the following is observed:

- Initially the AMW decays faster and to smaller values as temperature increases. This can be explained by the fact that as temperature increases, more TNT molecules have enough kinetic energy to overcome the decomposition barrier.
- At later times, it is seen that temperature increase speeds up the clusters formation. In addition, larger clusters are formed at a given time as temperature increases.

This temperature dependence can be understood by the increased mobility of the clusters at high temperatures, which allows them to diffuse and react faster.

The above temperature effect on clustering is observed at higher densities as well, as can be seen in Figure 14 (right) for the 30% compression case and $C \geq 7$. However, the initial decay of the AMW for $C \geq 7$, due to the decomposition of TNT molecules to smaller gaseous fragments, is almost negligible, even at the higher temperatures. This suggests that compression suppresses the detachment of small fragments, while clustering becomes favorable. The increased cluster formation is also seen for $C \geq 14$ and $C \geq 21$ (not shown). As explained above, the oscillations that appear in the decay of the AMW for $C \geq 0$ at 30% compression originate from the numerical instability of the clusters formed at that stage.

4.2. Pressure Effect on Clustering. The AMW dependence on compression ($C \geq 0$ and $C \geq 7$) is plotted in Figure 15 for 2250 (left) and 3500 K (right).

For $C \geq 0$ (inner panels) at both temperatures (2250 K, 3500 K) it is seen that the AMW reduces monotonically with time for the lower densities (ambient density and 15% compression); however, for 30% compression, a nonmonotonic behavior is observed. The latter behavior is correlated with the instability of clusters discussed above. It seems that the influence of compression on the decay is not significant in the case of $C \geq 0$. This density dependence differs from the one seen in Section 3.1 for the liquid TNT molecules decay (see Figure 4), where the decay speeds up with compression.

At both temperatures and $C \geq 7$ the clustering is enhanced as density rises: The clusters are formed sooner and reach a higher AMW value, at any given time. As previously mentioned, the initial AMW decay for $C \geq 7$ is suppressed when the density increases.

4.3. Kinetic Analysis. A possible mechanism to describe the cluster growth shown in Figure 13, during liquid TNT decomposition, is a stepwise mechanism, where the cluster size

dx.doi.org/10.1021/jp404907b | J. Phys. Chem. C 2013, 117, 21043−21054

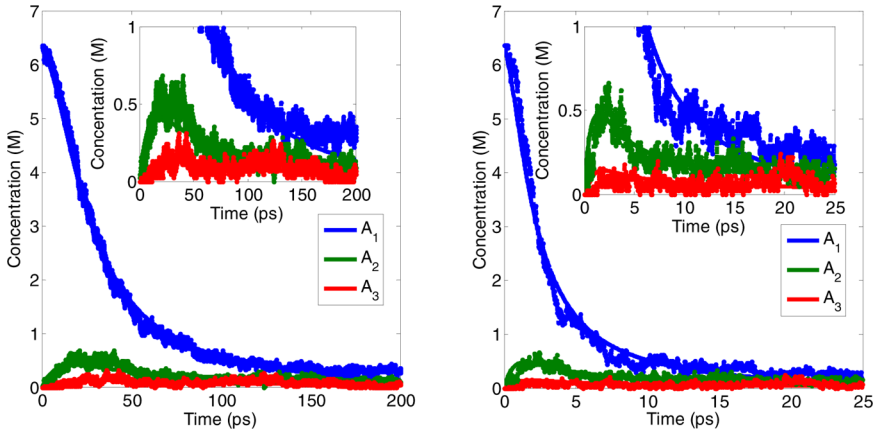

Figure 16. Temporal evolution of clusters A_1, A_2, and A_3 concentration (with $6 \le C \le 8$, $13 \le C \le 15$, $20 \le C \le 22$, respectively) at ambient density in the MD simulation (dashed lines) and in the linear growth kinetic model (full lines). Two temperatures are shown: 2250 (left) and 3500 K (right).

increases by approximately the MW of a single TNT molecule at each step. Such a linear growth model is applied below for the carbon clustering in hot liquid TNT decomposition. The model denotes the building block of the different clusters produced as A_1, which is defined as all fragments with $6 \le C \le 8$ carbon atoms. In general, A_i is defined as a fragment with $7i - 1 \le C \le 7i + 1$ carbon atoms, where $1 \le i \le 6$. (i is an integer.) k_i is the rate constant for the reaction between A_i and A_1, producing A_{i+1}. The kinetic model for the initial five clustering reactions is represented by the following equations:

$$A_1 + A_1 \xrightarrow{k_1} A_2$$

$$A_2 + A_1 \xrightarrow{k_2} A_3$$

$$A_3 + A_1 \xrightarrow{k_3} A_4$$

$$A_4 + A_1 \xrightarrow{k_4} A_5$$

$$A_5 + A_1 \xrightarrow{k_5} A_6$$

The kinetic model suggested produces a set of differential equations that cannot be solved analytically. To fit this kinetic model to the liquid TNT simulations results, the following numerical scheme is used:

- An initial guess for the rate constants in the above clustering reactions is made.
- A_i concentrations (denoted C_i) are calculated from the fragments analysis results of the MD simulations, using $C_i = n_f^i / N_A V$, where n_f^i is the number of fragments of type A_i, N_A is Avogadro's number, and V is the simulation cell volume.
- The set of five differential equations is numerically solved, producing the temporal variation of $A_i(t)$.
- A least-squares fitting to the MD simulation results is performed for only the three smallest clusters (A_1, A_2, and A_3), as for $i \ge 4$ $A_i \approx 0$ is obtained, and the clusters A_1, A_2, and A_3 are insensitive to the values of A_4–A_6.

The quality of fitness of the model, R^2, is evaluated by:

$$R^2 = 1 - \frac{\sum_{i,j} (N_i^{\mathrm{m}}[t_j] - N_i^{\mathrm{s}}[t_j])^2}{\sum_{i,j} (N_i^{\mathrm{m}}[t_j] - \overline{N_i^{\mathrm{s}}})^2}$$

where $N_i^{m/s}[t_j]$ is the number of fragments A_i at time t_j, obtained from the kinetic model result (m) or the MD simulation (s). $\overline{N_i^{\mathrm{s}}}$ is the time average of $N_i^{m/s}[t_j]$ for a given A_i.

In Figures 16 and 17, the linear growth model results are compared with the simulations results for ambient density at

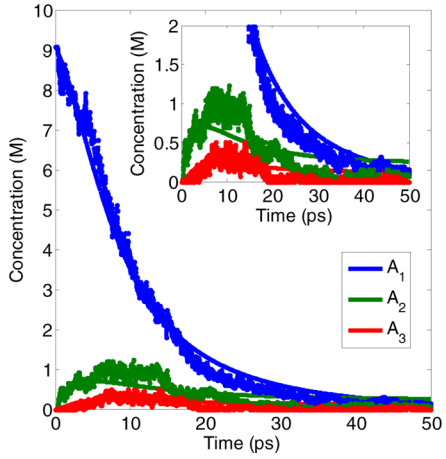

Figure 17. As Figure 16, for results at 2250 K and 30% compression.

2250 and 3500 K and for 30% compression at 2250 K, respectively. It is seen that, in general, there is a good agreement between the model and the simulation results for the clusters A_1–A_3. In particular, the agreement is very good at ambient density (at both temperatures shown in Figure 16) and is reasonable for the higher compression, which may indicate that a more complex clustering mechanism takes place as density increases. This agreement shows that the carbon clustering reactions and kinetics in hot, dense liquid TNT can be fairly described by the simple linear cluster growth model suggested here.

The rate constants k_1–k_3 obtained for various temperatures and compressions are shown in Table 6. As expected, increasing the temperature and pressure speeds up the clusters formation rate.

5. CONCLUSIONS

We validate that the first-principles-based ReaxFF reactive force field provides sufficient accuracy in the description of the fundamental reaction processes. The calculated results show that

dx.doi.org/10.1021/jp404907b | J. Phys. Chem. C 2013, 117, 21043–21054

Table 6. Rate Constants and Error Estimates Calculated with the Linear Growth Kinetic Model under Various Conditions

T [K]	V/V_0	k_1 [s^{-1} M^{-1}]	k_2 [s^{-1} M^{-1}]	k_3 [s^{-1} M^{-1}]	R^2
2250	1	0.0017	0.0171	0.0507	0.99
2700	1	0.0049	0.0525	0.1571	0.99
3500	1	0.0246	0.2111	0.6925	0.98
2250	0.85	0.0023	0.0205	0.0517	0.98
2250	0.7	0.0047	0.0395	0.1109	0.98

the overall thermal decomposition kinetics of hot, dense liquid TNT matches available macroscopic observations. This allows us to understand the atomistic origin of these reactions.

The structure of liquid TNT shows partial long-range order when prepared from the measured TNT crystal geometry. This order vanishes when preparing the liquid from an amorphous crystal. The liquid-cell geometry, however, has only a small influence on the liquid TNT decomposition process. The liquid structure should be further studied in the vicinity of TNT melting both experimentally and in simulations.

The thermal decomposition process of liquid TNT was analyzed starting from the initial, endothermic stage, through clusters formation, and reaching stable gaseous products.

A density dependence of the liquid TNT decomposition mechanism was observed:

- Initial reaction: The initial decomposition of ambient density liquid TNT begins with C−N bond scission (NO_2 release), whereas the dominant initial step of compressed liquid TNT is TNT dimer formation and decomposition to TNT derivatives.
- Clusters formation: Carbon clustering increases, while the small gases production is suppressed when the pressure and density rise.

The density-dependent initial decomposition path has an imprint on the density-dependent activation energy. The activation energy for the initial decomposition stage of ambient density liquid TNT is close to the measured value and is ∼25 kcal/mol lower than the corresponding (NO_2 homolysis) gas-phase unimolecular reaction barrier.

The temperature also influences the reaction path: At low temperatures (1800 K), the dimer formation and decomposition is the dominant initial decomposition path for all compressions studied. As temperature increases, the initial reaction path is determined by the liquid density, as described above. In addition, the temperature increase speeds up both the clustering reactions and the small fragments formation.

A linear growth kinetic model was suggested for the clustering process. The model was shown to be in a very good agreement with the simulation results at low compression and in reasonable agreement for 30% compression and 3500 K. At higher densities a more complex model may be required for describing the clustering in liquid TNT.

The stable gases production was calculated and compared with experimental data. A good agreement was obtained for N_2 and H_2O. The amount of carbon-containing gases (CO and CO_2) is underestimated in the simulations. The hydrogen-containing gases (H_2 and NH_3) are also lacking with respect to measurements but to a lesser extent. This difference is attributed to the inaccurate description of the soot production process in the simulations because the ReaxFF potentials were not yet trained for the clustering phenomena.

The decomposition process of solid TNT, under conditions similar to the ones used above for liquid TNT, is studied by Furman et al. in ref 17. At these high temperatures and pressures there are only slight differences, mainly in the initial decomposition steps, between the liquid and the solid TNT behavior.

■ ASSOCIATED CONTENT

Supporting Information

Amorphous liquid TNT preparation and thermal decomposition, pressure and PE evolution, bond order cutoff values, fragments analysis: initial and intermediate reactions, and ReaxFF parameters used in this study. This material is available free of charge via the Internet at http://pubs.acs.org.

■ AUTHOR INFORMATION

Corresponding Author

*E-mail: nomir@fh.huji.ac.il. Tel: 972-2-658-5485.

Notes

The authors declare no competing financial interest.

■ ACKNOWLEDGMENTS

S.Z. and W.A.G. were supported by the US ONR (N0014-12-1-0538 and N00014-09-1-0634). R.K. and Y.Z. acknowledge partial support of The Center of Excellence for Explosives Detection, Mitigation and Response, Department of Homeland Security.

■ REFERENCES

(1) Cohen, R.; Zeiri, Y.; Wurzberg, E.; Kosloff, R. Mechanism of Thermal Unimolecular Decomposition of TNT (2, 4, 6-trinitrotoluene): a DFT Study. *J. Phys. Chem. A* **2007**, *111*, 11074−11083.

(2) Rom, N.; Zybin, S. V.; van Duin, A. C. T.; Goddard, W. A.; Zeiri, Y.; Katz, G.; Kosloff, R. Density-Dependent Liquid Nitromethane Decomposition: Molecular Dynamics Simulations Based on ReaxFF. *J. Phys. Chem. A* **2011**, *115*, 10181−10202.

(3) Plimpton, S. Fast Parallel Algorithms for Short-Range Molecular Dynamics. *J. Comput. Phys.* **1995**, *117*, 1−19. LAMMPS web site: http://lammps.sandia.gov.

(4) van Duin, A. C. T.; Dasgupta, S.; Lorant, F.; Goddard, W. A. ReaxFF: A Reactive Force Field for Hydrocarbons. *J. Phys. Chem. A* **2001**, *105*, 9396−9409.

(5) van Duin, A. C. T.; Strachan, A.; Stewman, S.; Zhang, Q. S.; Xu, X.; Goddard, W. A. ReaxFFSiO Reactive Force Field for Silicon Oxide Systems. *J. Phys. Chem. A* **2003**, *107*, 3803−3811.

(6) Liu, L.; Liu, Y.; Zybin, S. V.; Sun, H.; Goddard, W. A. ReaxFF-lg: Correction of the ReaxFF Reactive Force Field for London Dispersion, with Applications to the Equation of State for Energetic Materials. *J. Phys. Chem. A* **2011**, *115*, 11016−11022.

(7) Hobbs, M. L.; Kaneshige, M. J.; Gilbert, D. W.; Marley, S. K.; Todd, S. N. Modeling TNT Ignition. *J. Phys. Chem. A* **2009**, *113*, 10474−10487.

(8) Zhang, L.; Zybin, S. V.; van Duin, A. C. T.; Dasgupta, S.; Goddard, W. A.; Kober, E. M. Carbon Cluster Formation during Thermal Decomposition of Octahydro-1,3,5,7-tetranitro-1,3,5,7-tetrazocine and 1,3,5-Triamino-2,4,6-trinitrobenzene High Explosives from ReaxFF Reactive Molecular Dynamics Simulations. *J. Phys. Chem. A* **2009**, *113*, 10619−10640.

(9) Chen, X. F.; Liu, J. F.; Meng, Z. H; Han, K. L. Thermal Unimolecular Decomposition Mechanism of 2,4,6-trinitrotoluene: a first-principles DFT Study. *Theor. Chem. Acc.* **2010**, *127*, 327−344.

(10) Carper, W. R.; Davis, L. P.; Extine, M. W. Molecular Structure of 2,4,6-Trinitrotoluene. *J. Phys. Chem.* **1982**, *86*, 459−462.

(11) Dobratz, B. M. Crawford, P. C. *LLNL Explosives Handbook: Properties of Chemical Explosives and Explosive Simulants*; Lawrence Livermore National Laboratory: Livermore, CA, 1985; Chapter I-8.5, Table 8-10.

(12) Tung, Y. S; Mu, R.; Ueda, A.; Henderson, D. O.; Curby, W. A.; Mercado, A. Diffusion Kinetics of TNT in Nitrile Rubber via FTIR-ATR Spectroscopy. *Internet J. Vib. Spectrosc.* **1998**, *1* (5), 58−67.
(13) Garn, W. B. Determination of the Unreacted Hugoniot for Liquid TNT. *J. Chem. Phys.* **1959**, *30*, 819−822.
(14) Davis, W. C.; Craig, B. G.; Ramsay, J. B. Failure of the Chapman-Jouguet Theory for Liquid and Solid Explosives. *Phys. Fluids* **1965**, *8*, 2169−2182.
(15) Guidry, R. M.; Davis, L. P. Thermochemical Decomposition of Explosives. I. TNT Kinetic Parameters Determined from ESR Investigations. *Thermochim. Acta* **1979**, *32*, 1−18.
(16) Pruitt, C. J. M; Goebbert, D. J. The C-N Dissociation Energies of Nitrobenzene and Nitrotoluene Radical Anions and Neutrals. *Chem. Phys. Lett.* **2013**, *580*, 21−27.
(17) Furman, D.; Kosloff, R.; Dubnikova, F.; Zybin S. V.; Goddard, W. A.; Rom, N.; Hirshberg, B.; Zeiri, Y., submitted.
(18) Ornellas, D. L. The Heat and Products of Detonation of Cyclotetramethylenetetranitramine, 2,4,6-Trinitrotoluene, Nitromethane, and Bis[2,2-dinitro-2-fluoroethyl]formal. *J. Phys. Chem.* **1968**, *72*, 2390−2394.
(19) Viecelli, J. A.; Glosli, J. N. Carbon Cluster Coagulation and Fragmentation Kinetics in Shocked Hydrocarbons. *J. Chem. Phys.* **2002**, *117*, 11352−11358.
(20) Chevrot, G.; Sollier, A.; Pineau, N. Molecular Dynamics and Kinetic Study of Carbon Coagulation in the Release Wave of Detonation Products. *J. Chem. Phys.* **2012**, *136*, 084506−10.
(21) Pineau, N.; Soulard, L.; Los, J. H.; Fasolino, A. Theoretical Study of Nucleation/Growth Process of Carbon Clusters Under Pressure. *J. Chem. Phys.* **2008**, *129*, 024708−8.
(22) Mcennis, C.; Dikmelik, Y.; Spicer, J. B. Femtosecond Laser-Induced Fragmentation and Cluster Formation Studies of Solid Phase Trinitrotoluene using Time-of-flight Mass Spectrometry Applied Surface Science. *Appl. Surf. Sci.* **2007**, *254*, 557−562.
(23) Emelianov, A.; Eremin, A. Detonation Wave Initiated by Explosive Condensation of Supersaturated Carbon Vapor Shock Waves. *Shock Waves* **2010**, *20*, 491−498.